Chapter 3
Data Processing

The methods developed in this book are used to calculate high rate position and orientation states of a moving body relative to the earth using a comprehensive sensor suite. Unfortunately, the different sensors move relative to each other and measure quantities along different, uncoupled axes. For example, the MotionPack's accelerometers measure acceleration and its rate gyros measure angular velocity along three perpendicular directions that move with the ship with the acceleration signals contaminated by gravitational acceleration, which is always orientated towards the center of the earth. Similarly, the TCM2 compass measures the heading of the moving body with respect to the magnetic North, and the tilt sensor measures the roll and pitch angles with respect to the ship. Conversely, the GPS computes geodetic latitude, longitude and height above sea level relative to the rotating earth. Therefore, the data measured from each one of the sensors need to be rotated into a common frame of reference. The first section of this chapter, section 3.1.1, defines the different reference frames used. The second section, section 3.2, derives the transformations necessary to convert vectors between the reference frames and into a common reference frame. The third section, section 3.3, describes the data fusion algorithm and its implementation. Finally, the last section, section 3.4, defines the method used to process the ADCP data.

3.1 Reference Frames

From the GPS geodetic data, the GPS position is calculated in the Earth-Centered Earth-Fixed frame, ECEF, described firstly in the following section. The GPS velocity is obtained using the ground speed and the course over ground provided by the GPS and expressed in the North-East-Down (NED) frame described secondly in the following section. In the NED frame is also expressed the TCM2 compass heading. The third section explains the body-fixed frame, where the tilt sensor, the IMU and the ADCP outputs.

C. Gelin: A Low-Cost, High Rate Motion Measurement System, NAMESS 1, pp. 19–35.
springerlink.com

3.1.1 Earth-Centered Reference Frames

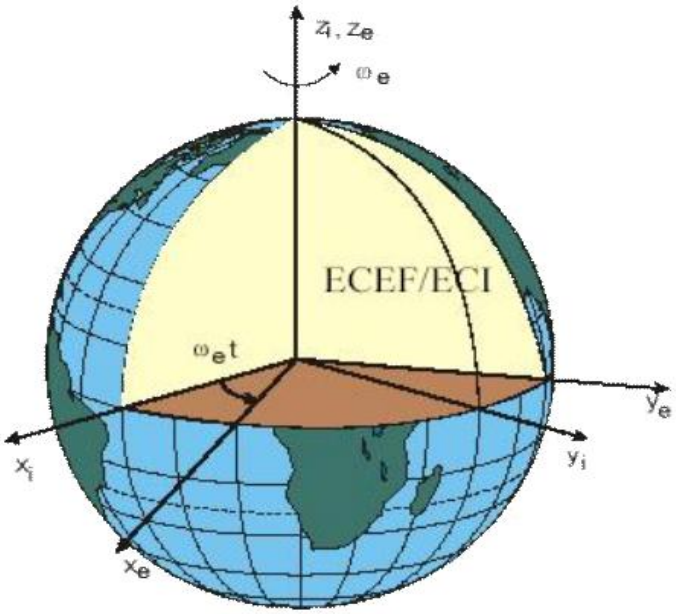

Fig. 18 Representation of the axis of the Earth Centered Earth Fixed and Earth Centered Inertial Frames

The Earth-Centered Inertial frame (ECI, *i-frame*) has its origin at the center of the earth, with axes $[X_i, Y_i, Z_i]^T$ that are non-rotating with respect to the fixed stars.The Earth-Centered Earth-Fixed (ECEF, e-frame) has its origin at the center of the earth, with axes [Xe, Ye, Ze]T fixed to the Earth that rotates at a rate of 15.041067 °/hr (7.2921.10-5 rad/s) with respect to the ECI. The Zi and Ze axes point from the center of the Earth upwards towards the North Pole. The Xi and Xe axes point horizontally in the plane of the equator from the center of the Earth towards the equator at zero latitude. The Yi and Ye axes are chosen to complete the right hand coordinate system (Figure 18). The ECI and ECEF frame are taken into account in the process of obtaining the GPS position data as described in section 3.2.1.

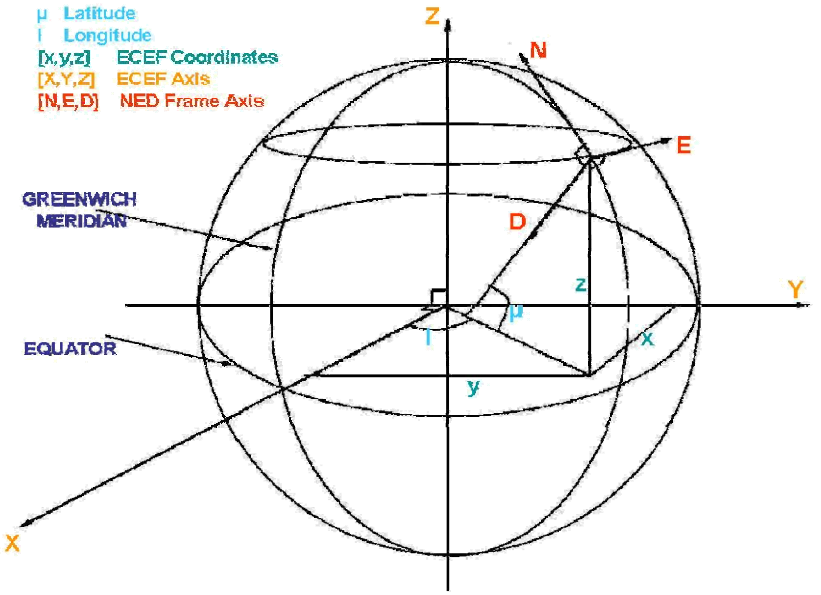

Fig. 19 Schematic representation of the North East Down reference frame

3.1.2 North East Down Reference Frame

Traditionally the North-East-Down (NED) coordinate system is local and is attached to Earth. Since the motion of the Earth has minimal effect on low speed marine vehicle, it is considered inertial. The NED coordinate system, $\Im_E$, has its origin at the location of the navigation system, where the *X*-axis points northward, the *Y*-axis points eastward, and the *Z*-axis points towards the center of the Earth (Figure 19). For marine vessels operating in a local area defined by only small variations in longitude and latitude, the location of an object is best expressed using NED coordinates (Fossen, 1994). The GPS position data are converted from the ECEF to the NED frame as described in section 3.2.1. The TCM2 compass heading is also expressed in $\Im_E$.

3.1.3 Body Fixed Reference Frame

The body-fixed frame, $\Im_B$, is a moving coordinate frame rigidly attached to either a ship or sensor package to which the sensors' axes of sensitivity are aligned. Traditionally, The *x*-axis points forward, the *y*-axis points starboard, and the *z*-axis completes a right-hand orthogonal system by pointing downward. The IMU, the tilt sensor and the ADCP uses this coordinate system as described in sections 3.2.2 and 3.2.3.

3.1.4 Vessel States

For a ship moving in six degrees of freedom (DOF), 6 independent states are necessary to define the position and orientate the vessel (Figure 20).

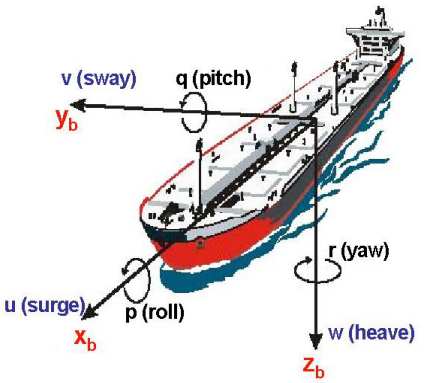

Fig. 20 Ship-fixed coordinate reference frame (red) and 6 degrees of Freedom motion variables for a marine vessel (sway, surge, heave, pitch, roll and yaw) (Fossen 1994)

These body fixed states are conveniently expressed in a vector representation with the position vector η:

$$\boldsymbol{\eta} \equiv [x, y, z]^{\mathrm{T}}\,, \tag{1}$$

where x, y and z denote the distances from the origin of $\Im_{\mathrm{B}}$ to the location of interest along the x, y and z axes respectively. Similarly, positions in $\Im_{\mathrm{E}}$ are:

$$\boldsymbol{H} \equiv [X, Y, Z]^{\mathrm{T}}. \tag{2}$$

From here on, capitalized letter represent variables expressed in the NED frame while the lower case variables represent variables expressed in the body fixed frame. The linear velocity vector v in the body frame is defined by

$$\dot{\boldsymbol{\eta}} = \boldsymbol{\nu} \equiv [u, v, w]^{\mathrm{T}}\,, \tag{3}$$

Where u is the velocity in the x-direction (surge), v is the velocity in the y-direction (sway), and w is the velocity in the z-direction (heave). The Euler angle rotations are defined as:

$$\boldsymbol{\beta} \equiv [\phi, \theta, \psi]^{\mathrm{T}}\,, \tag{4}$$

Where ϕ is the roll about the x-axis, θ is the pitch about the y-axis, and ψ is the yaw about the z-axis (Figure 20). The angular velocity in the body fixed frame is defined as:

$$\boldsymbol{w} \equiv [p, q, r]^{\mathrm{T}}\,, \tag{5}$$

Where p is the angular velocity about the x-axis, q is the angular velocity about the y-axis, and q is the angular velocity about the z-axis.

3.2 Coordinate Transformation

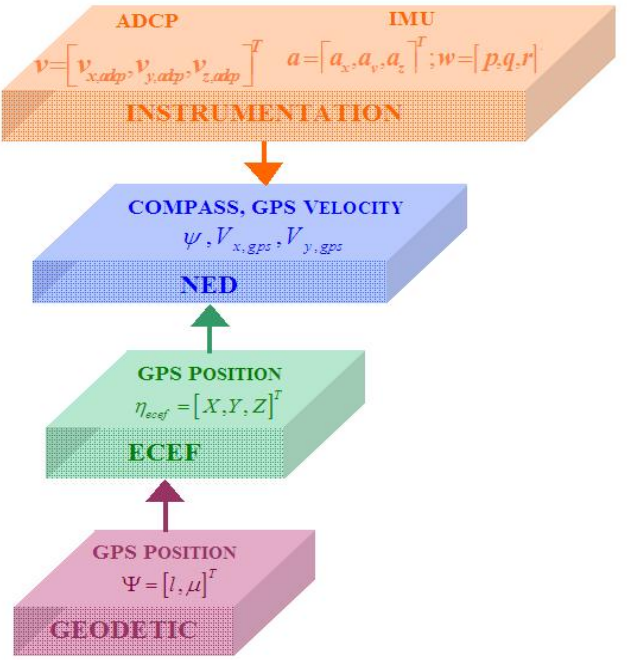

Fig. 21 Diagram of the sensors output variables and the coordinate transformations

The following section describes the transforms used to rotate data from the different sensor frames to the NED reference frame, the common frame of reference (Figure 21).

3.2.1 Transformation from Geodetic to ECEF and from ECEF to NED

The GPS measures the geodetic latitude and longitude of the vessel in an Earth-Centered Inertial frame (ECI). To be useful for local positioning, this measure must be transformed into the NED local reference frame (Figure 21).

The Geodetic latitude, μ, and longitude, l, provided by the GPS are first transform to the ECEF coordinate system. Latitude and longitude are provided in the geodetic datum on which the GPS calculations are based, WGS-84 (World Geodetic System 1984). The transformation from the geodetic coordinates $\boldsymbol{\psi} = [l, \mu]^{\mathrm{T}}$ for a given height h to the ECEF position $\boldsymbol{H}_{ecef} \equiv [X_{ecef}, Y_{ecef}, Z_{ecef}]^{\mathrm{T}}$ is:

$$\begin{pmatrix} X_{ecef} \\ Y_{ecef} \\ Z_{ecef} \end{pmatrix} = \begin{pmatrix} (N+h).\cos(\mu).\cos(l) \\ (N+h).\cos(\mu).\sin(l) \\ [N.(1-e^2)+h].\sin(\mu) \end{pmatrix}, \quad (6)$$

Where N is the prime vertical radius of curvature (Figure 22) given by: $N = a/\sqrt{1-[e^2 * \sin^2(\mu)]}$, h is the height above ellipsoid, e^2 = 0.00669437999013 is the eccentricity squared, a = 6378137m is the semi major earth axis (ellipsoid equatorial radius), and b = 6356752.3142m is the semi minor earth axis (ellipsoid polar radius). Figure 22 represents the Ellipsoid parameters, prime vertical radius of curvature (N), ellipsoid equatorial radius (a), ellipsoid polar radius (b), height above ellipsoid (h), geodetic latitude (ϕ), and geodetic longitude (λ). Q represents a point at the surface of the Earth and P a point at a height h above Q.

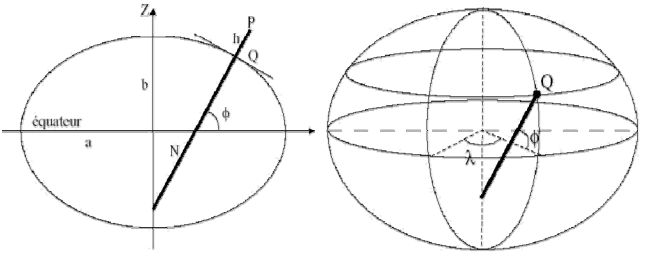

Fig. 22 Representation of the Ellipsoid parameters

Once the position vector is converted to the ECEF coordinate system, a transformation matrix is applied to align the position vector with the NED reference frame.

The transformation matrix T_{ecef}^{ned} is (Fossen 1994):

$$T_{ecef}^{ned} = \begin{bmatrix} -\sin(\mu)\cos(l) & -\sin(\mu)\sin(l) & \cos(\mu) \\ -\sin(l) & \cos(l) & 0 \\ -\cos(\mu)\cos(l) & -\cos(\mu)\sin(l) & -\sin(\mu) \end{bmatrix}, \tag{7}$$

Where the position vector in the NED frame is:

$$\boldsymbol{H} = T_{ecef}^{ned} H_{ecef}. \tag{8}$$

3.2.2 Transformations from Component Reference Systems to Body Fixed Reference System

The IMU and the ADCP output data along axes that are defined relative to their individual orientation. Often because the axes of the instruments may not be aligned with the axes of the ship, this data needs to be rotated and translated to the ship fixed frame prior to transformation to the NED frame. For example, accelerations measured using the IMU are transformed to the body fixed frame using:

$$\begin{pmatrix} a_{x,B} \\ a_{y,B} \\ a_{z,B} \end{pmatrix} = T_{IMU}^{body} \begin{pmatrix} a_{x,IMU} \\ a_{y,IMU} \\ a_{z,IMU} \end{pmatrix}, \tag{9}$$

Where $a_{x,B}$, $a_{y,B}$, and $a_{z,B}$ represents the accelerations in the ship fixed frame, $a_{x,IMU}$, $a_{y,IMU}$, and $a_{z,IMU}$, the accelerations in the IMU body fixed frame, and $T_{IMU}^{body} \equiv [-1,1,-1]^{\mathrm{T}}$ in this application.

3.2.3 Transformations from Body Fixed Frame to NED

Measurements made or converted into the body-fixed representation are converted into the NED (the common) reference frame to simultaneous compare and process the signals. Sequential *Z*, *Y*, *X* Euler angle transformation is used to transition between the body fixed and the NED frames. This transformation is not based on a physical orientation but strictly on a set of sequential rotations (Etkin 1972). The rotation between the ship body fixed frame and the NED frame is:

$$T_{body}^{ned} = \begin{bmatrix} \cos\theta\cos\psi & [\cos\psi\sin\theta\sin\phi - \sin\psi\cos\phi] & [\cos\psi\sin\theta\cos\phi + \sin\psi\sin\phi] \\ \cos\theta\sin\psi & [\cos\psi\cos\theta + \sin\phi\sin\psi\sin\phi] & [\sin\psi\sin\theta\cos\phi - \cos\psi\sin\phi] \\ -\sin\theta & \cos\theta\sin\phi & \cos\theta\cos\phi \end{bmatrix}. \quad (10)$$

The inverse transformation from the NED frame to the body frame is:

$$T_{body}^{ned} = \begin{bmatrix} \cos\theta\cos\psi & \cos\theta\sin\psi & -\sin\theta \\ [\cos\psi\sin\theta\sin\phi - \sin\psi\cos\phi] & [\cos\psi\cos\theta + \sin\phi\sin\psi\sin\phi] & \cos\theta\sin\phi \\ [\cos\psi\sin\theta\cos\phi + \sin\psi\sin\phi] & [\sin\psi\sin\theta\cos\phi - \cos\psi\sin\phi] & \cos\theta\cos\phi \end{bmatrix}. \quad (11)$$

Unfortunately rotational velocities in the body fixed frame do not directly measure the Euler rates; instead they measure angular velocities about a fixed set of axes. These angular rates do not constitute a vector space and therefore can't be integrated to provide a measure of orientation. Thus, the angular rates are converted to Euler rates using:

$$\Gamma = \begin{bmatrix} 1 & \sin(\phi)\tan(\theta) & \cos(\phi)\tan(\theta) \\ 0 & \cos(\phi) & -\sin(\phi) \\ 0 & \frac{\sin(\phi)}{\cos(\theta)} & \frac{\cos(\phi)}{\cos(\theta)} \end{bmatrix}, \quad (12)$$

where the Euler rates are found by:

$$\dot{\beta} = \begin{pmatrix} \dot{\phi} \\ \dot{\theta} \\ \dot{\psi} \end{pmatrix} = \Gamma \begin{pmatrix} p \\ q \\ r \end{pmatrix} = \Gamma \dot{w}, \quad (13)$$

where the dot above the variable $(\cdot)$ represents a time derivative, $\frac{d(\cdot)}{dt}$.

3.3 Data Fusion

Consider the measurements $x_m(t)$ and $\dot{x}_m(t)$ of some state $x(t)$ output by two distinct sensors (position sensor and velocity sensor for example). In navigation and positioning applications, the measurement, $x_m(t)$, is often accurate and stable,

but the update is slow and the resolution coarse. The derivative measurement $\dot{x}_m(t)$ is often high frequency, but is subject to a bias that results in drift of the integrated signal. Thus, each one of these signals cannot be used independently for applications that require high quality navigation data. However, they have complementary characteristics that can be leveraged to obtain a combined useful signal. The data fusion techniques developed in this work combine the complementary outputs of sensors measuring a related state to eliminate the drift of integrating the measurement $\dot{x}_m(t)$, while increasing the rate and resolution of $x_m(t)$. The pre-emphasized signal, $x_p(t)$, is obtained by summing the signal $x_m(t)$ with the derivative signal $\dot{x}_m(t)$, such that (Mudge and Lueck 1994):

$$x_p(t) = x_m(t) + \frac{1}{\Omega_c}\dot{x}_m(t)\ , \tag{14}$$

where the scaling factor Ω_c , denoting the cutoff frequency, is a real positive constant. The choice of Ω_c is determined by the characteristics of the complementary region of the two sensors. For frequencies that are small compared to the cutoff frequency ($\Omega \ll \Omega_c$), the signal portion of the spectrum comes predominantly from $x_m(t)$, while for $\Omega \gg \Omega_c$), the signal is predominately from $\dot{x}_m(t)$. In the frequency domain, the pre-emphasized signal $x_p(t)$ is:

$$X_p(\Omega) = \left(1 + \frac{i\Omega}{\Omega_c}\right) X(\Omega), \tag{15}$$

Where $X(\Omega)$ is the Fourier transform of the signal $x(t)$. The enhanced version $x_e(t)$ of the signal $x(t)$ is then obtained by convolving $x_p(t)$ with a single-pole, low-pass filter having the transfer function:

$$H(\Omega) = \frac{1}{1+\frac{i\Omega}{\Omega_c}}\ , \tag{16}$$

yielding:

$$X_e(\Omega) = X_p(\Omega)H(\Omega) = \left(\left(1 + \frac{i\Omega}{\Omega_c}\right) X(\Omega)\right)\left(\frac{1}{1+\frac{i\Omega}{\Omega_c}}\right), \tag{17}$$

where Ω_c can now be interpreted as the half-power cutoff frequency of $H(\Omega)$. The enhanced signal $x_e(t)$ of the signal $x(t)$ contains low-frequency information from the sensor measuring $x_m(t)$, and the high-frequency information from the sensor measuring $\dot{x}_m(t)$.

3.3.1 Data Fusion Overview

Prior to processing and fusing any translational measurements, they first need to be rotated to the NED frame using the Euler angles, which are not directly measured. Compounding this problem is that the Euler angles are implicit in the

matrix $\Gamma(12)$, converting angular rates to Euler rates, and thus, they need to be known *a priori* to calculate $\dot{\beta}$ from w (13). The Euler angles, β, are obtained by merging the low-frequency Euler angles, θ_L, and ϕ_L, calculated from the tilt measurements ξ and ζ, and the compass heading, ψ_L, with the high-frequency IMU angular rates, $\boldsymbol{w} \equiv [p, q, r]^{\mathrm{T}}$. The estimated Euler angles are then used to convert the IMU acceleration from body-fixed frame, $\boldsymbol{a} \equiv [\dot{u}, \dot{v}, \dot{w}]^{\mathrm{T}}$, to the NED frame, $\boldsymbol{A} \equiv [\ddot{X}, \ddot{Y}, \ddot{Z}]^{\mathrm{T}}$, where gravity is removed and the signal is merged with the GPS velocity, $[\dot{X}_{LF}, \dot{Y}_{LF}, \dot{Z}_{LF}]$. The result of the last data fusion leads to a high quality merged measure of the ship's velocity $\equiv [V_X, V_Y, V_Z]$.

3.3.2 Estimation of the Euler Angles

The angular rate sensors of the IMU are not fixed and they are subject to a low frequency drift. Therefore, these sensors cannot be directly integrated to calculate an accurate long-term measure of the angular position. Instead, they are merged with the tilt sensor and compass measurements that provide a low frequency measure of the roll, pitch, and yaw Euler angles. However, the tilt sensor does not directly measure the Euler angles but measures the angle between gravity and its axes of sensitivity and the relationship between the Euler angles and the tilt measurements ξ and ζ is

$$\theta_L = \zeta \ , \tag{18}$$

and

$$\phi_L = \operatorname{asin}\left(\frac{\sin \xi}{\cos \zeta}\right) \tag{19}$$

The Euler angles calculated from the tilt sensor data were calibrated using the accelerometers. This was done using an accelerometer to measure acceleration along its axis of sensitivity and at frequencies where the translational acceleration of the IMU is negligible so that the accelerometers only measure gravity. Thus, at low frequencies, with little translational motion, the accelerometers can provide an independent measure of the Euler angles, (Figure 23), (Lueck, Nahon 2000):

$$a_{x,L} = -g \sin \theta_L \ , \tag{20}$$

and

$$a_{y,L} = g \cos \theta_L \sin \phi_L \tag{21}$$

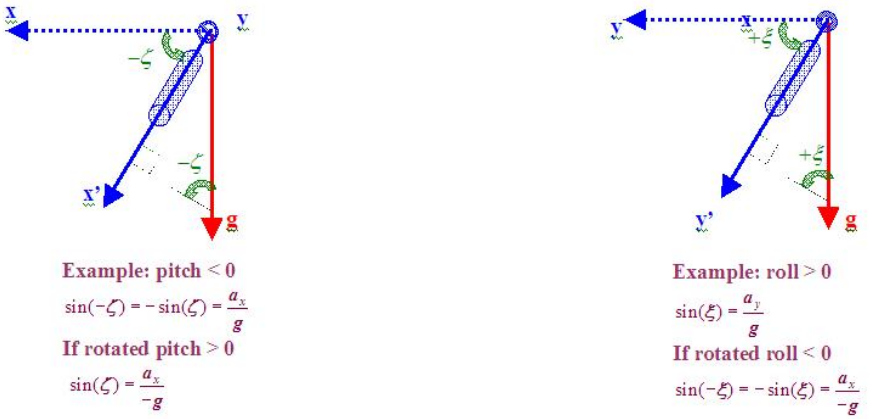

Fig. 23 Acceleration measurements in function of the rotation angles

To compare the angular measurements of the tilt sensor with these of the accelerometer, the IMU and tilt sensor were mounted on the same rigid plate and very slowly rotated through the expected tilt range. Data for each sensor was simultaneously acquired and recorded (Figure 24). The vessel is expected to rotate less than 20°, and within this range, the angles measured by both the sensors agree within ± 0.54366° for ϕ and within ± 0.48737° for θ. At angles greater than 30°, the accuracy of the tilt sensor decreases with range. At the maximum tilt of 42°, the tilt sensor overestimated the tilt by up to 10° and this difference results because of the non-linear response of the tilt sensor, which can be corrected for using a calibration table. When the tilt sensor is steady, local vibrations can cause the fluid to slosh; this coupled with processes internal to the sensor causes a ± 1.1541° fluctuation in the tilt measurements. The tilt sensor can only provide reliable data at frequencies less than 1Hz and higher frequency signal is removed by applying 1st order Butterworth low-pass filter at a cutoff frequency of 1Hz to the tilt sensor roll, ξ, and pitch, ζ.

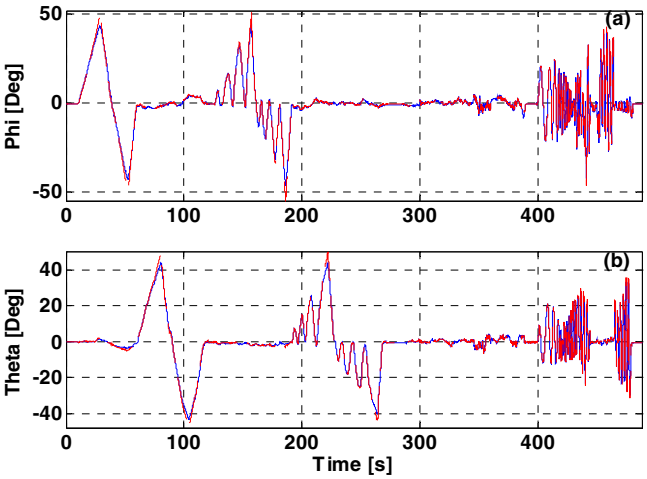

Fig. 24 Comparison between the low frequency estimates of Euler angle ϕ_L(a) (θ_L(b)) obtained from the IMU (blue) and from the Tilt sensor (red).

The TCM2 compass provides a direct measure of the yaw Euler angle, ψ, but similar to the tilt sensors, it also has a finite response time and sudden changes in heading cannot be directly measured with this instrument. Thus, only the low-frequency yaw signal is useful and the low-frequency estimate of ψ, ψ_L, is obtained by applying a 1st order Butterworth low-pass filter to the compass heading, ψ_{CP} with a cut-off frequency of 1Hz.

At higher frequencies (> 1/30Hz) the rotation rates, $\boldsymbol{w} \equiv [p, q, r]^{\mathrm{T}}$ measured with the IMU provide the needed angular measurements, $\dot{\boldsymbol{\beta}}_{\boldsymbol{H}} \equiv [\dot{\phi}_H, \dot{\theta}_H, \dot{\psi}_H]^{\mathrm{T}}$, that are used as angular derivative signal in the data fusion. The compass, tilt sensor and IMU signals are combined to create the pre-emphasized signal $\boldsymbol{\beta}_{\boldsymbol{P}} \equiv [\phi_H, \theta_H, \psi_H]^{\mathrm{T}}$, according to (14):

$$\phi_P = \phi_L + \frac{1}{\Omega_C}\dot{\phi}_H \,, \tag{22}$$

$$\theta_P = \theta_L + \frac{1}{\Omega_C}\dot{\theta}_H \,, \tag{23}$$

and

$$\psi_P = \psi_L + \frac{1}{\Omega_C}\dot{\psi}_H. \tag{24}$$

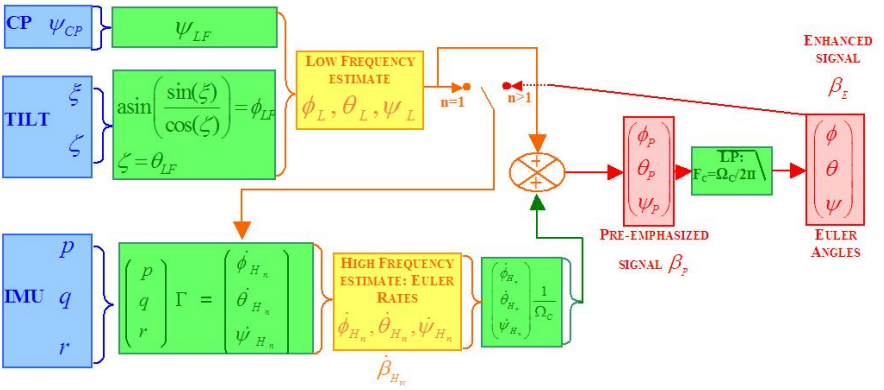

Fig. 25 Diagram of the data fusion IMU / TCM2/ Tilt sensor to obtain Euler angles, β.

The pre-emphasized signal β_P contains the low-frequency information from the tilt sensors (ϕ_L, θ_L) and from the compass (ψ_L) and the high-frequency information from the rate gyros, β_P is convolved with a 1st order Butterworth filter with a cutoff frequency F_C to calculate the Euler angles, $\boldsymbol{\beta_E} \equiv [\phi, \theta, \psi]^{\mathrm{T}}$ using (17). The Butterworth filter is selected because it has a more linear phase response in the passband compare to other filters like Chebyshev and Elliptic filters. The Euler rates are calculated from the angular rates using (13). Unfortunately, implicit in Γ in (12) are the Euler angles ϕ and θ that are not known at high frequency. Therefore, an iterative method is used to accurately compute the Euler rates. In the first iteration (n=1), the Euler angles at low-frequency, ϕ_L, θ_L are used to estimate Γ, yielding an initial estimate of $\dot{\beta}_{H_n}$, $\dot{\boldsymbol{\beta}}_{\boldsymbol{H_1}} \equiv [\dot{\phi}_{H_1}, \dot{\theta}_{H_1}, \dot{\psi}_{H_1}]^{\mathrm{T}}$ (Figure 25). The first estimate for β_E is then used to transform the angular rates to Euler rates to obtain a second estimate of $\dot{\beta}_{H_n}$ which is merged with β_L, to provide a more accurate second measure of β_E, (Figure 25), and so forth. Values for the Euler angles converged to within 1×10^{-11}° after only three iterations, and therefore, this is the number of iterations performed.

The IMU rate gyros have a low drift rate and the data fusion point is chosen to be at 1/30Hz. This data fusion frequency is selected so that at frequencies lower than the cutoff frequency, the tilt sensors and compass heading, provide accurate and stable measures of the Euler angles, ϕ, θ and ψ and at frequencies above the cutoff frequency, the rate gyros in the IMU provide accurate measures of the Euler rates, $\dot{\phi}$, $\dot{\theta}$ and $\dot{\psi}$.The method of merging the data from tilt sensor, compass, and IMU rate gyros to calculate the Euler angles is verified for 3 sets of motions:

1. Turning the system slowly clockwise then anticlockwise through a range of different angles for each axis of rotation,
2. Turning the system slowly anticlockwise, then clockwise 360° around the Z-axis, and
3. Turning the sensor system simultaneously about multiple axes and rotation.

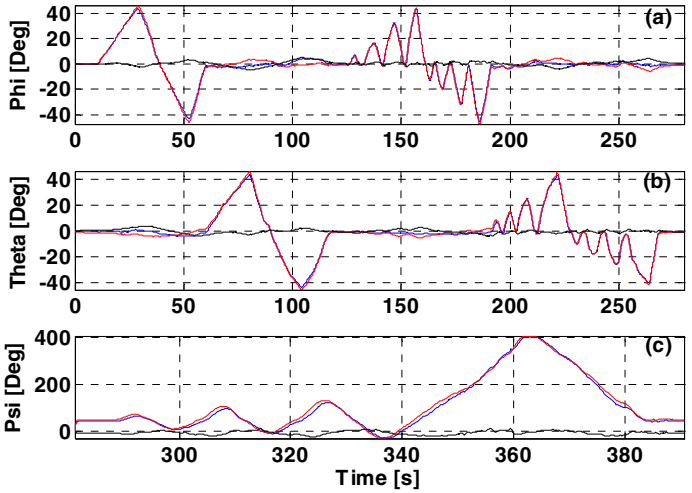

Fig. 26 Comparison between the Euler angles ϕ_L (a), θ_L (b) from accelerometers, blue and ϕ (a), θ (b) from data fusion, red and between the compass heading, blue and Euler angle ψ from data fusion in red (c). The black is the difference of blue and red signals.

To quantify the accuracy of the merged Euler angle signals at lower frequencies (< 5 Hz), they are compared with an independent measure of the Euler angles calculated using the accelerometer (Figure 26) for motion set 1. Figure 26 shows the comparison between the Euler angle ϕ_L from the accelerometers in blue and ϕ from Data fusion, red (a) from the first part of the test. On the second panel (b), from the first part of the test, the Euler angle θ_L from accelerometers in blue is compared to θ from the data fusion in red. Finally, on the last panel (c), from the second part of the test, the unwrapped heading from compass is in blue, and ψ from Data fusion is in red. The black is the difference of the merged and IMU Euler angle. During the post processing, a low-pass filter (cutoff at 1 Hz) is applied to both the Euler angles derived from the IMU and the Euler angles obtained by the data fusion and the standard deviation of their difference is ± 1.9° for ϕ, ± 1.5° for θ (most likely due to inaccuracy of the tilt sensor pass 30°) and ± 8° for ψ.

The raw signals are filtered both prior to and during data fusion and this creates a frequency dependant phase distortion. Thus, to quantify any potential signal delay, the cross-correlation between the Euler angles measured strictly with the accelerometer are compared to the merged Euler angle estimates and normalized so that the autocorrelations at zero lag are identically to 1.0. Comparing the Euler angles from the accelerometer and from the data fusion, ϕ_L and ϕ are 99.23% correlated with a delay of 7 samples (0.0547s), θ_L and θ are correlated at 99.66% and delayed by 11 samples. The compass heading and ψ correlate at 99.38% with no delay. The compass is a digital serial device that is first processed and coded into RS-232 format at the compass, broadcast, then received and processed by the data acquisition computer. Any delay is due to the lag associated with this overhead and should be accounted for within the motion correction of the ADCP although in our case an agreement of more than 99% is considered acceptable.

To validate the high frequency component of β_E (Figure 25), the Euler rates β_H are integrated and compared to the Euler angles, β_E, yield through the data fusion (Figure 27). The figure shows the third part of the test during the high frequency set of motion. In the first panel (a), the high frequency component of the integral of Euler rate $\dot{\phi}$, blue, is compared to the high frequency component of the merged Euler angle ϕ, red. In the 2nd panel (b), the high frequency component of the integral of Euler rate $\dot{\theta}$, blue, is compared to the high frequency component of the merged Euler angle θ, red and in the last panel (c), the high frequency component of the integral of Euler rate $\dot{\psi}$, blue, is compared to high frequency component of the merged Euler angle ψ, red. The black is the difference of the two signals in each plot.

As expected, the difference between directly integrating β_H yields to a low frequency drift. The standard deviation is ±0.44° for ϕ, ± 0.38° for θ and ± 0.58° for ψ. To quantize the phase agreement between the Euler rates and the Euler angles, the corresponding cross-correlations are computed, $\dot{\phi}$ and ϕ are 99.99% correlated with no delay, $\dot{\theta}$ and θ are correlated at 99.99% with no delay. Looking at the first 10s of Figure 27 third panel (c) the high frequency component of the integral of Euler rate $\dot{\psi}$ is not following the same behavior of the high frequency component of the merged Euler angle ψ. This is due to the high-pass filtering process itself and leads to $\dot{\psi}$ and ψ being delayed by 4 samples and 84.30% correlated.

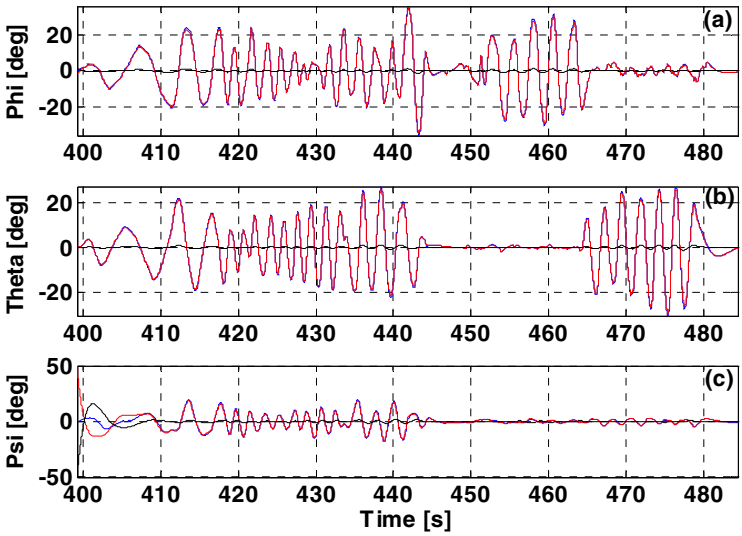

Fig. 27 During the third part of the test, high frequency set of motion, comparison between the high frequency component of the integral of Euler rate $\dot{\phi}$ (a), $\dot{\theta}$ (b), $\dot{\psi}$ (c) in blue, and the high frequency component of the merged Euler angle ϕ (a), θ (b) and ψ (c) in red. The black is the difference of the two signals in each plot.

The distribution of variance with frequency (the power spectral distribution) of the merged tilt sensor, compass, and IMU gyros is also verified by comparing $FFT(\beta_E)$ with $FFT(\beta_L)$, for low frequency and with $FFT(\beta_H)$ for high frequency. Below the data fusion point, 1/30Hz, the spectra of the merged Euler angles match the spectra of the low-frequency estimates of the Euler angles, and above the data fusion point, they match the spectra of the Euler rates (Figure 28).

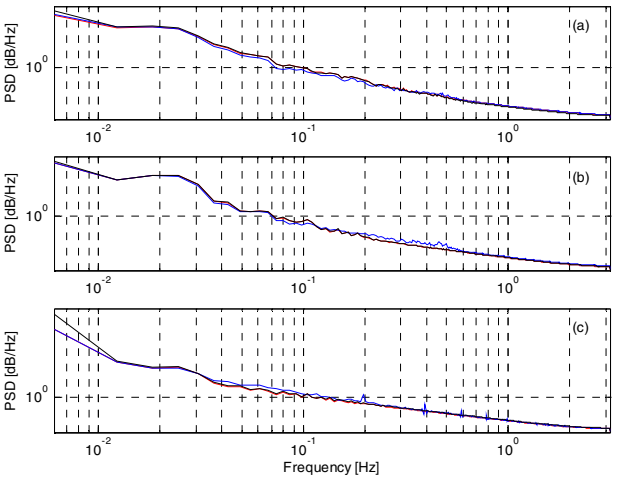

Fig. 28 In red, PSD of Merged Euler angle ϕ (a), θ (b) and ψ (c); in blue, PSD of Euler angle from tilt sensor ϕ_L (a), θ_L (b), and ψ_L(c); in black, PSD of integrated Euler rate $\dot{\phi}$ (a), $\dot{\theta}$ (b), and $\dot{\psi}$ (c).

3.3.2.1 Estimation of the Ship's Velocity and Position

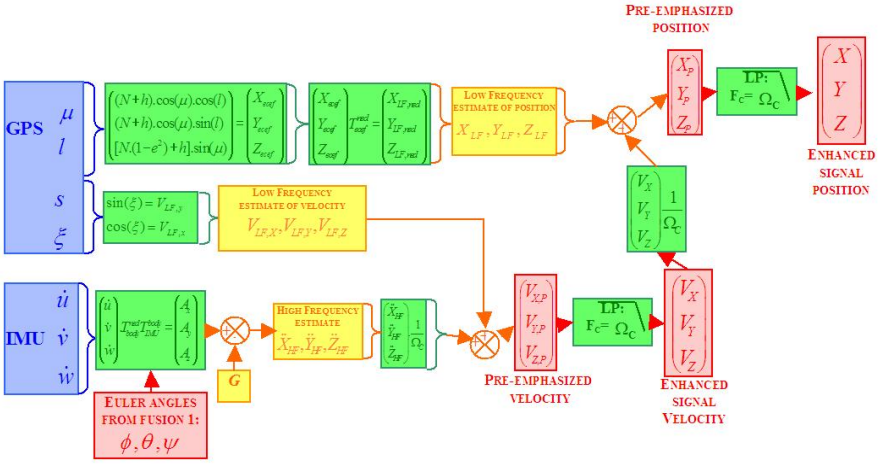

Fig. 29 Diagrammatic representation of the data fusion of the IMU data and the GPS data used to obtain the ships velocity V.

The enhanced velocity of the ship, $\boldsymbol{V}$, is obtained by directly fusing the high frequency (128Hz) acceleration measurement from the IMU, $\boldsymbol{A^{IMU}}$, and the low frequency (0.5Hz) velocity obtained from the speed and course overground output from the GPS, $\boldsymbol{V_{LF}^{GPS}} \equiv [V_{LF}^X, V_{LF}^Y, V_{LF}^Z]^{\mathrm{T}}$(Figure 29). For this calculation, the accelerations are rotated to the NED frame from its instrumentation frame and the gravitational contamination is removed,

$$\boldsymbol{A^{IMU}} = T_{body}^{ned} T_{IMU}^{body} \boldsymbol{a^{IMU}} - \boldsymbol{G} \text{ where } \boldsymbol{G} = [0\ 0\ g]^{\mathrm{T}}. \tag{25}$$

The $\boldsymbol{V_{LF}^{GPS}}$ and $\boldsymbol{A^{IMU}} \equiv [\ddot{X}_{HF}, \ddot{Y}_{HF}, \ddot{Z}_{HF}]^{\mathrm{T}}$ are then combined to create the pre-emphasized velocity $\boldsymbol{V_P}$ using (14):

$$V_P^X = V_{LF}^X + \frac{1}{\Omega_C} \ddot{X}_{HF}, \tag{26}$$

$$V_P^Y = V_{LF}^Y + \frac{1}{\Omega_C} \ddot{Y}_{HF} \tag{27}$$

and

$$V_P^Z = V_{LF}^Z + \frac{1}{\Omega_C} \ddot{Z}_{HF} \tag{28}$$

After this, $\boldsymbol{V_P}$ is to be convolved with a 1st order Butterworth filter with a cutoff frequency Ω_C to obtain the full frequency measure of the ships velocity, $\boldsymbol{V_E}$, according to (17).

The position is then obtained by merging the enhanced velocity, $\boldsymbol{V} \equiv [V_X, V_Y, V_Z]^{\mathrm{T}}$, with the latitude and longitude measured with the GPS. The latitude and longitude, measured by the GPS, are converted to NED position measurements using (6) and (8),

$$\boldsymbol{H^{GPS}} = T_{ecef}^{ned} \boldsymbol{H_{ecef}^{GPS}}. \tag{29}$$

3.4 ADCP Processing

The ADCP consists of four transducers tilted at equal angles (20°) from the vertical axis of the ADCP in a convex configuration and oriented in pairs that point in perpendicular planes (Figure 30). The ADCP reference frame (x_{adcp}, y_{adcp}, z_{adcp}) has its origin at the center of the ADCP, where the four transducers intersect. The axes x_{adcp} and y_{adcp} are coplanar with the horizontal ship plane and the x_{adcp}-axis points from port to starboard and the y_{adcp}-axis points from stern to bow. The z_{adcp}-axis points positive upward.

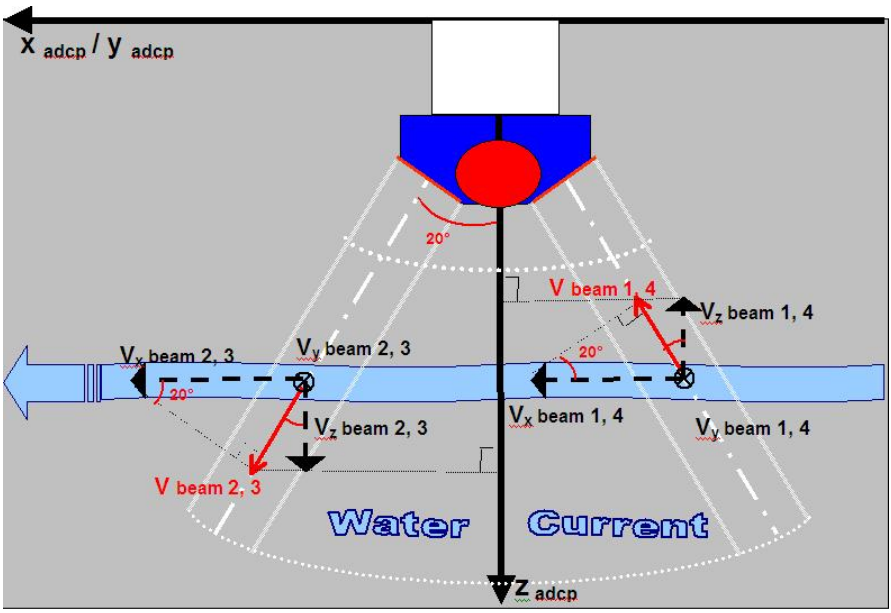

Fig. 30 ADCP beam and reference frame

Assuming that the water velocity is horizontally homogenous but varies vertically within the beam envelope of the ADCP, the three orthogonal relative water velocity components *u*, *v*, and *w* in the ADCP reference frame are

$$u_i = \frac{V_{i,beam1} - V_{i,beam2}}{2 * \sin(20°)} = 1.4619(V_{i,beam1} - V_{i,beam2}), \tag{30}$$

$$v_i = \frac{V_{i,beam4} - V_{i,beam3}}{2 * \sin(20°)} = 1.4619(V_{i,beam4} - V_{i,beam3}), \tag{31}$$

and

$$w_i = \frac{V_{i,beam1} + V_{i,beam2} + V_{i,beam3} + V_{i,beam4}}{4 * \cos(20°)} \tag{32}$$

$$= 0.2666(V_{i,beam1} + V_{i,beam2} + V_{i,beam3} + V_{i,beam4}).$$

where the index *i* is the number of the bin, each bin representing a different depth cell of the profiled water column, from 1 to 128 in our case. The Earth fixed water velocity of bin *i* is obtained using the body to inertial transformation matrix L_{IB} and subtracting the measured velocity of the ship,

$$\boldsymbol{V_i} = L_{IB} \begin{bmatrix} u_i \\ v_i \\ w_i \end{bmatrix} - \boldsymbol{V_{ship}}. \tag{33}$$